Effects of Al_2O_3 addition on microstructure and luminescence of transparent germanosilicate glass-ceramics with incorporated spinel Ga-oxide nanocrystals

N.V.Golubev[a], E.S.Ignat'eva[a] ,A.S.Lipatiev[a], M.Z.Ziaytdinova[ab], G.I.Lapushkin[c] ,V.N.Sigaev[a], M.V.Poliakov[d], A. Paleari[ae], R. Lorenzi[e]

[a] *P.D. Sarkisov International Laboratory of Glass-based Functional Materials, Mendeleev University of Chemical Technology of Russia, 9 Miusskaya Square, 125047 Moscow, Russia*

[b] *P.N. Lebedev Physical Institute of the Russian Academy of Sciences, 53 Leninskii pr., 119991 Moscow, Russia*

[c] *Moscow Institute of Physics and Technology (MIPT), 9 Institutskiy per., 141700 Dolgoprudny, Russia*

[d] *Institute of Nanotechnology of Microelectronics of the Russian Academy of Sciences, 32A Leninsky Prospekt, 119991 Moscow, Russia*

[e] *Department of Materials Science, University of Milano-Bicocca, Via Cozzi 55, 20125 Milano, Italy*

Abstract

Ga-oxide spinel nanocrystals are wide band gap systems, which can be incorporated in a glass matrix by phase separation mechanisms. In suitable conditions, this kind of processes can give rise to transparent nanostructured glass-ceramics with UV excitation and luminescence properties potentially interesting in several technological areas. Nanophase size dispersion and volume fraction have been demonstrated to be controllable, at some extent, by suitable thermal treatments for nucleation and nano-crystallization in low-alkali gallium germanosilicate system. Here we report the results on the role of Al_2O_3 additions on the microstructure and optical response of the glass-ceramics fabricated in this system. Data of differential scanning calorimetry, X-ray diffraction, transmission electron microscopy, absorption and fluorescence spectroscopy show that Al_2O_3 addition, up to 4.5 mol%, turns out to have a considerable impact on the size and number density of precipitated nanocrystals, which are solid solutions of γ-$Ga_{2-x}Al_xO_3$ resulting from the partial incorporation of Al^{3+} ions into the crystalline phase. We show that the use of

Al_2O_3 as an additive in the composition of gallium germanosilicates facilitates glass melting and leads to glass-ceramics with significantly modified photoluminescence characteristics such as decay lifetime and integrated intensity of light emission. The possible reasons are discussed.

Keywords:

Optical properties; Glass ceramics; Spinels; Al_2O_3

1. Introduction

Additive compounds in glass technology are known to have a great impact on glass crystallization, structure and properties of fabricated glass-ceramics (GCs), depending on the glass composition and the type and concentration of the dopant species [1,2]. Relatively high amounts of additives could drastically change the composition of precipitating crystalline phases and hence the sequence of phase transformations [[3], [4], [5]]. In contrast, lower additive concentrations (up to several mol%) do not alter, as a rule, the phase development but either noticeably promote crystallization process or inhibit nucleation and growth kinetics [[6], [7], [8]]. Consequently, through this kind of effects, additives can also play a role in controlling the incorporation of own ions or ions of other dopants into precipitating crystals for the implementation and optimization of luminescence properties and related spectral features. In particular, the properties of light emission in low-alkali gallium silicate glasses were extensively studied for the selective embedding of Ni [9], Cr [10], Cr and Ni [11], Co [12], Mn [13] or rare-earth [14] ions into the nanocrystals (NCs) of Ga-oxide phases. At the same time, considerably less attention has been given to the intrinsic photoluminescence of Ga-oxide nanophase, including spinel-like γ-Ga_2O_3 NCs, grown in silicate glass matrix [15,16]. These NCs are responsible for a broad luminescence band in the blue region at around 450 nm, ascribed to the radiative recombination of donor and acceptor pairs (DAPs) [17]. Importantly, luminescence kinetics, stability and thermal evolution of Ga-oxide nanophases in an amorphous matrix turn out to be largely different with respect to the freestanding and pure compound [18,19]. Much of the interest in such transparent GC materials comes from an

intense UV-C excited light emission, which makes the fabrication of solar-blind UV-to-visible optical converters possible [18,20]. However, the task of optimizing the light output of these converters by an improved control over nanostructure formation still remains a challenge.

As regards the possible additives in this perspective, Al_2O_3 seems to be the most convenient compound among common oxides, which can alter the microstructure or, more strictly speaking, sub-microstructure of GCs with Ga-oxide phases, without changing the sequence of phase transformations. Microstructure modifications can in fact be induced at least as a result of viscosity change upon Al_2O_3 addition. Furthermore, no relevant change in the sequence of phase transformations is expected even at a relatively high Al_2O_3 content because of the similar structural role of Ga and Al ions in silicate glasses [[21], [22], [23]]. However, Al_2O_3 addition (above the starting composition) increases the molar ratio R_2O_3/Me_2O (R = Ga, Al; Me = Li, Na) and can provide alkali gallium silicate glasses with a higher propensity to crystallization and a larger resulting fraction of crystalline phase. Importantly, the spectral distribution of luminescence is not expected to be drastically modified by the additional component – so preserving the main features of large Stokes shift between excitation and emission – since the incorporation of Al^{3+} in γ-Ga_2O_3 NCs should not lead to the formation of new defect sites and localized states associated with charge compensation. As a matter of fact, Al_2O_3 is quite common as a component of low-alkali Ga-containing silicate oxide glasses doped with transition metal ions [11,13,[24], [25], [26]] but practically without mentioning its role in the fabrication and optical response of such GCs except for some rare publications [16,27]. In regard to the studies focused on the effect of Al_2O_3 content on the intrinsic luminescence of NCs in similar undoped glasses, they are practically lacking. Some data on Al_2O_3 impact on the microstructure and optical properties of gallium silicate GCs are given in a recent paper by Lin et al. [16]. The authors used a broad concentration range of Al_2O_3 (5–20 mol%), which was added by the partial substitution of Ga_2O_3 in the glass composition. However, limited attention has been paid to the effects of Al_2O_3 addition on the DAP luminescence in transition metal-free samples. Actually, at the moment, there are few contradictory data in the literature, reporting either lower [16] or higher [28] integrated luminescence intensity than in Al_2O_3-free GCs.

The aim of the present paper is to give a comprehensive experimental basis and interpretation of the effects of Al_2O_3 addition to the light emission properties of Ga-oxide nanophase in alkali-germanosilicate GCs comprising a thorough study of luminescence intensity and decay kinetics, glass crystallization, Ga-oxide nanophase composition and a change in the microstructure of fabricated GCs, in a composition series with Al_2O_3 content ranging from 0 to up to 4.5 mol% over 100%.

2. Experimental

Glasses with nominal molar composition $7.5Li_2O$-$2.5Na_2O$-$20Ga_2O_3$-$35GeO_2$-$35SiO_2$ doped with different Al_2O_3 content were prepared using special purity grade amorphous SiO_2 (Ltd «Lanthan center for technology», Moscow, Russia), GeO_2 (JSC «Germanium», Krasnoyarsk, Russia), chemically pure Li_2CO_3 and Ga_2O_3 (Ltd «Rare Metals Plant», Koltsovo, Russia), Na_2CO_3 and analytical grade $Al(OH)_3$ (Ltd «JSC Reachem», Moscow, Russia). Al_2O_3 was introduced in an amount of 1.5, 2.5, 3.5 and 4.5 mol% over 100%; Al-free glass was also synthesized for comparison purpose. The appropriate proportions of the raw materials were calculated in order to prepare 30 g of the final product. These materials were weighed with an accuracy of 0.001 g and then were hand mixed for 10 min. The batches were melted in a Pt crucible at 1480 °C for 1 h using a home-made electrically heated furnace. The melt was cast onto a stainless-steel plate and quenched by being pressed with another stainless-steel plate to obtain ~2.5 mm thick samples. Their visual inspection revealed that the addition of Al_2O_3 led to some phase separation on the surface of the castings. Importantly, when increasing Al_2O_3 content, the glass forming ability appeared to be continuously decreased as evidenced by the growth of phase separation zones on the surface presumably identified as γ-Ga_2O_3-based solid solutions and some amount of Al-doped gallium germanate phase with mullite structure. To avoid nucleation risks, the parent glasses were not annealed after quenching. The most homogeneous parts of the parent glasses were then cut and prepared as necessary for further analyses. The surface phase separation was mechanically removed before any measurements were performed. The glass and GC samples were labelled in

accordance with Al_2O_3 amount in the composition of glasses, i.e. 0Al (corresponds to Al-free sample), 1.5Al (corresponds to the sample with 1.5 mol% Al_2O_3), etc.

Differential scanning calorimetry (DSC) was performed by means of a thermal analyzer STA 449 F3 Jupiter (Netzsch, Germany) in a Pt crucible, at a heating rate of 10 °C/min in Ar, on bulk samples of 25.5 ± 0.3 mg. An empty Pt pan was used as a standard. The glass transition temperature (T_g) was determined as the extrapolated onset of the transition, while exopeak (T_{exo}) and endopeak temperatures (T_{endo}) were defined as the peak extremum temperature in DSC curves. The values of T_g were reproducible to within ±3 °C for all the fabricated glasses, while those for T_{exo} were precise to ±3 and ± 7 °C for several samples cut from each casting of Al-doped and Al-free glasses, respectively.

The parent glasses were heat-treated in a furnace Vario 200 (Zubler, Germany) at 640 °C, with an accuracy of temperature control within ±1 °C, to obtain transparent GCs. The samples of similar weight ($\Delta m \leq 0.25$ g) were placed into the furnace directly at the treatment temperature, and after holding for 15 min, they were immediately removed from the furnace.

The density of the parent glasses and GCs was determined at room temperature by Archimedes method with distilled water as an immersion liquid. Density measurements of a silica glass sample were accurate to within ±0.01 g/cm^3 when determined by the same apparatus.

X-ray diffraction (XRD) patterns of powdered samples were recorded by means of a diffractometer D2 Phaser (Bruker, Germany) employing nickel-filtered CuKα radiation. To perform Rietveld-based quantitative phase analysis, 7 wt% of CaF_2 (special purity grade, Ltd «JSC Reachem», Moscow, Russia) was added to the parent glassy and GC powders. CaF_2 was also used as an internal standard for *d*-spacing measurements. The final samples were prepared by weighing the appropriate amounts of the components and carefully mixing them in ethanol along with additional grinding to less than 10 μm using an agate mortar and a pestle. The mixtures were dried at room temperature in air for ~30 min and were analyzed on the same day. XRD data were collected between 10 and 100° 2θ, with a step size of 0.02° and a counting time of 1.5 s per step. To reveal solid solution formation between Ga- and Al-oxide phases and estimate a mean crystallite size

with higher precision, the XRD peak at about 64.2° was measured with a counting time of 9 s per step. The crystallite size was evaluated with an uncertainty of about 5% from the half-width of the diffraction maximum by using Scherrer equation. In calculation, Scherrer constant was assumed to be 0.9 [29]. Crystalline phases were identified by comparing the peak position and relative intensities in the X-ray diffraction patterns with the ICDD PDF-2 database (release 2011).

The crystalline and glassy phase weight fractions were extracted by Rietveld refinement strategy employing PONKCS (Partial or No Known Crystal Structure) procedure [30]. In order to obtain empirical calibration constant *ZMV* (*ZM* and *V* – the mass and volume of the unit cell, respectively) of the residual glass in fabricated GCs, «*hkl* phases» were developed for an amorphous phase by using the samples consisting of the known amount of CaF_2 and one of the corresponding parent glasses. The difference in X-ray scattering efficiency of the parent and residual glasses was neglected. This is a reasonable assumption since the crystalline phase content in fabricated GCs is relatively low. The instrumental background profile was determined from the X-ray scan of an empty silicon-made low-background specimen holder. The values of atomic coordinates and initial unit-cell parameters were taken from Ref. [31] and Ref. [32] for γ-Ga_2O_3 and CaF_2, respectively. The fitting of the X-ray diffraction patterns was performed by software TOPAS 4.2 (Bruker, Germany).

Transmission electron microscopy (TEM) and electron diffraction patterns of the parent glasses were obtained on a finely ground powder using a microscope JEM-2100 (JEOL, Japan) with an accelerating voltage of 200 kV. TEM and high angle annular dark field scanning TEM (HAADF-STEM) images as well as electron diffraction patterns of GC samples were obtained on a finely ground powder with the help of a microscope Titan G2 60–300 (FEI/Thermo Fisher, USA) operating at an accelerating voltage of 300 kV and equipped with an energy-dispersive X-ray (EDX) detector system. No effect of electron irradiation on the samples was observed during the low-resolution TEM study. Measurements of not less than 500 nanoparticles (NPs) were made from various regions of the sample to establish NC size distribution in fabricated GCs. The analysis of TEM images was performed with DigitalMicrograph software (Gatan, USA). The mean NP size

corresponding to arithmetic mean length size was calculated from a particle size distribution given as a histogram [33].

Optical absorption spectra were collected on well-polished samples ~2 mm in thickness using a spectrophotometer UV-3600 (Shimadzu, Japan). Photoluminescence (PL) and PL-excitation (PLE) patterns were obtained as contour plots of light intensity by collecting PL spectra, with 10 nm of bandwidth for excitation and emission, with the help of a spectrofluorimeter Cary Eclipse (Varian, USA). The uncertainty of the relative PL intensity from excitation and light collection reproducibility in steady-state measurements is less than 10%.

PL decay kinetics were investigated in three different time regimes: nanosecond (500 ns range), microsecond (10 μs) and millisecond (1 ms). The decay curves in the ns and μs regimes were recorded by means of a fluorescence spectrometer FLS900 (Edinburgh Instruments, UK) with a pulsed LED source at 250 nm as an excitation source (pulse width 920 ps) and with the emission monochromator at 450 nm (20 nm of bandwidth). PL decay measurements in the ms regime were collected with the spectrofluorometer Cary Eclipse exciting at 250 nm (10 nm of bandwidth) by means of a pulsed xenon lamp and integrating the signal in a range of 20 nm at around 450 nm, with a delay from the pulse of 0.1 ms and a resolution of 1 μs. The data have been fitted as a sum of three (ns and μs regimes) or two (ms regime) exponentials, without taking into account the convolution with the instrument response function since the fastest time regime was an order of magnitude longer than the LED pulse. Mean lifetime values were calculated as described in [34].

$$<\tau>=\sum a_i\tau_i^2/\sum a_i\tau_i ,$$

where α_i is the pre-exponential factors in a multi-exponential intensity decay, τ_i – the fluorescence lifetime of the *i-th* discrete component and $\Sigma\alpha_i = 1.0$.

3. Results and discussion

3.1. Thermal evolution of parent glasses

The DSC curves of Al-free and Al-doped glasses have similar features and are shown in Fig. 1. For all the glasses, only one crystallization exopeak is exhibited due to the formation of a single Ga-oxide spinel phase. It is identified as γ-Ga_2O_3 in the case of Al-free glass composition studied previously [19] and γ-Ga_2O_3-based solid solutions for Al-doped glasses as will be shown later in section 3.2. There is a clear influence of Al_2O_3 on the values of T_g and T_{exo}. In fact, the addition of Al_2O_3 results in a shift of T_g and T_{exo} to higher and lower values, respectively, compared to Al-free glass (Fig. 1). Higher values of T_g, implying the increase of the low-temperature viscosity when the molar ratio $Ga_2O_3/(Ga_2O_3+Al_2O_3)$ decreases, have indeed been previously reported for the glasses in the system Li_2O-$(Ga,Al)_2O_3$–SiO_2 [35] in the restricted range of molar ratio $(Ga_2O_3+Al_2O_3)/Li_2O \leq 1$. No systematized data are at the moment available for Al-doped glasses neither in gallium silicate systems at molar ratio greater than 1 nor in studied gallium germanosilicate system. The value of T_g is known to be linked to cation coordination number, cross-link density and tightness of packing of an oxide network [36]. Higher values of these factors lead to an increase of T_g. Within a narrow concentration range of doping, far from the equivalence point where $R_2O_3/Me_2O = 1$ (R = Ga, Al; Me = Li, Na), no coordination changes should be encountered, taking also into account that the possible existence of octahedrally coordinated Ga (Al) and Ge ions in similar silicate and germanate glasses remains controversial, and these ions predominantly occupy tetrahedral sites in the glass network [22,23,[37], [38], [39], [40]]. As for the cross-link density, it seems to be even decreased at least due to the lower relative content of the glass-forming oxides after Al_2O_3 addition. To compare the tightness of packing of the oxide network, the oxygen packing density or the volume occupied by 1 mol of oxygen can be calculated from the density of a glass and its composition [41]. The molar volume of oxygen turns out to be decreased for the parent glasses from 13.44 (Al-free) to 13.27 cm^3 (4.5Al) suggesting that T_g increase is mainly associated with the change of the oxygen density.

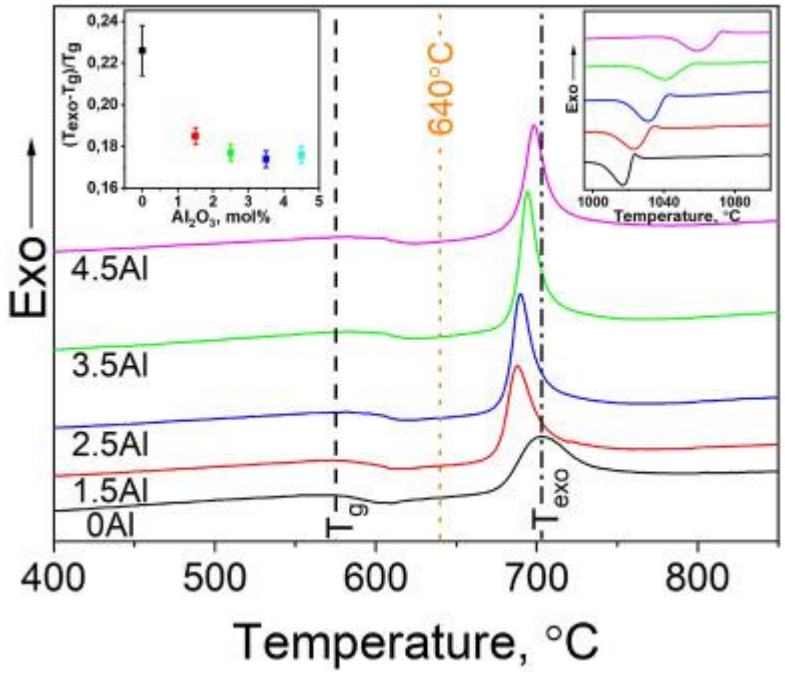

Fig. 1. DSC curves (vertically shifted for clarity) of the parent glasses. Black dashed and dash-dotted lines represent the position of glass transition (T_g) and exopeak extremum temperature (T_{exo}) for Al-free glass, respectively. Orange dotted line indicates the treatment temperature. The inset on the left displays the influence of Al_2O_3 content on the difference between T_{exo} and T_g weighted by $1/T_g$, and the inset on the right shows the high-temperature part of the DSC curves. (For interpretation of the references to colour in this figure legend, the reader is referred to the Web version of this article.)

As regards to the lowered T_{exo} values compared to T_{exo} for Al-free glass, they lead to a shortened T_{exo}-T_g range, which indicates decreased glass resistance against devitrification. Comparing the fabricated glasses with different T_g by means of the factor $(T_{exo}-T_g)/T_g$ [42], we in fact find that the crystallization tendency on heating is definitely higher in all Al-doped glasses (Fig. 1, left inset) above the uncertainty in the values of T_g and T_{exo} for several samples from the same melt. This conclusion is also supported by the fact that crystallization occurs in a narrower temperature range for these glasses, and the exothermic peaks are sharper and more intense, pointing to larger crystallization rates after Al_2O_3 addition. Moreover, a higher propensity to the crystallization is consistent with the observation that glass forming ability is progressively reduced by increasing Al_2O_3 content (see experimental section) since a positive correlation exists between glass stability and glass forming ability [43]. According to a simple structural model, such non-isothermal

crystallization behaviour can be explained by an increase of R_2O_3/Me_2O molar ratio or, if we assume a larger preference for Al^{3+} to occupy tetrahedral sites in the glass network [23], by Ga_2O_3/Me_2O one (R = Ga, Al; Me = Li, Na). As a matter of fact, the formation of $[AlO_4]^-Me^+$ tetrahedral units needs alkali ions, and hence less of these ions become available to balance the local charge of gallium-oxygen tetrahedra. As a result, Ga_2O_3/Me_2O ratio increases, and phase separation is intensified both during melt quenching and in the subsequent heat treatment of the glasses. Here, attention should be given to a nonmonotonic trend in the change of the crystallization tendency: it increases up to 2.5–3.5 mol% Al_2O_3 and then slightly decreases. The origin of this different behaviour in 4.5Al glass can be explained by an even minor amount of NCs possibly precipitating on quenching in the glass with the highest content of Al_2O_3 and the influence of crystallization beginning on the position of T_g and T_{exo} [44]. The exopeak area is in fact decreased when moving from the DSC curve of 3.5Al glass to the curve of 4.5Al sample (Fig. 1), and XRD analysis confirms the presence of a minor fraction of crystalline phase in the latter glass (Fig. S1).

Regarding the dispersion of T_g and especially T_{exo} values noted above, it is worth to be mentioned that scatter of them is slightly but noticeably less in Al-doped glasses than in Al-free glass. Greater dispersion of indicated values in later glass is likely caused by extended chemical inhomogeneities probably due to incomplete homogenization of the melt as a result of its rather high viscosity. However, we should emphasize that our Al-free glass according to its XRD and electron diffraction patterns (Fig. S1, S2) was amorphous and without any inclusions of unmelted batch. As for Al-doped glasses, even a moderate fall in the liquidus temperature can improve – at constant melting conditions – melt homogeneity and can result in a more homogeneous glass at the macroscale. This temperature fall is in fact expected when the number of glass components increases because of a sort of weakening of the germanosilicate networking propensity when Si(Ge)-*O*-Si(Ge) bonds are replaced by weaker Si(Ge)-*O*-Al ones [45,46]. Consequently, overall chemical homogeneity of Al-doped glasses at macroscale should be improved even if they demonstrate the phase separation on the surface and become more inhomogeneous at sub-microscopic level as a result of pronounced tendency towards devitrification.

Another fact deserving consideration is the growth of the extremum temperature of the endopeak (Fig. 1, right inset) previously ascribed to the decomposition of the spinel phase $LiGa_5O_8$, formed from γ-Ga_2O_3 NCs, in the glass of Al-free composition [19]. Taking into account the occurrence of solid solutions in the $LiGa_5O_8$–$LiAl_5O_8$ system [47] and the higher thermal stability of $LiAl_5O_8$ [48] compared to $LiGa_5O_8$ [49], such a growth of the endopeak temperature is the first evidence of Al^{3+} incorporation in the crystalline Ga-oxide phases precipitated in the fabricated glasses. Indeed, the position of Bragg reflections in the XRD patterns of 4.5Al GCs is shifted to larger diffraction angles – also after treatment above T_{endo} – compared to Al-free GCs (Fig. S3), and it can be considered as a strong indication of the solid solution formation. As regards the mechanisms potentially responsible for slowing down $Li(Ga,Al)_5O_8$ precipitation and decomposition, we cannot completely exclude, however, the formation of diffusion barriers around NCs [50] that suppresses crystal growth and tendency to decompose with lithium release.

3.2. XRD and TEM of heat-treated glasses

Based on the DSC curves and our previous data on similar glass compositions [28,51], the heat treatment at 640 °C for 15 min was performed on all the fabricated glasses. Fig. 2 displays the XRD patterns of Al-free and Al-doped GCs and also Al-free parent glass as a reference. The XRD patterns of all the parent glasses show the typical feature of an amorphous phase, except for 4.5Al glass, whose XRD pattern registers a minor amount of Ga-oxide spinel phase precipitated in the bulk (Fig. S1). Sharp diffraction peaks in Fig. 2 and S1 correspond to CaF_2 added to all the samples to reveal the shift of Bragg reflections of the embedded Ga-oxide spinel phase and to perform Rietveld-based quantitative phase analysis. The heat treatment leads to bulk precipitation of a crystalline phase with broad Bragg reflections, which are indicative of the small size of the precipitated NCs. Scherrer analysis of the peak broadening gives estimated crystallite sizes (Table S1) ranging from ~5 nm (Al-free) to ~4 nm (Al-doped). The analysis of the Al_2O_3 dependent broadening of the XRD reflection at about 64.2° in GC samples registers the most relevant NC size reduction after the first Al_2O_3 addition (1.5Al sample) and a minor further decrease (as will

be confirmed later in section 3.4) with 2.5 mol% Al_2O_3. Greater Al_2O_3 addition does not cause further relevant changes of NC size above the experimental uncertainty.

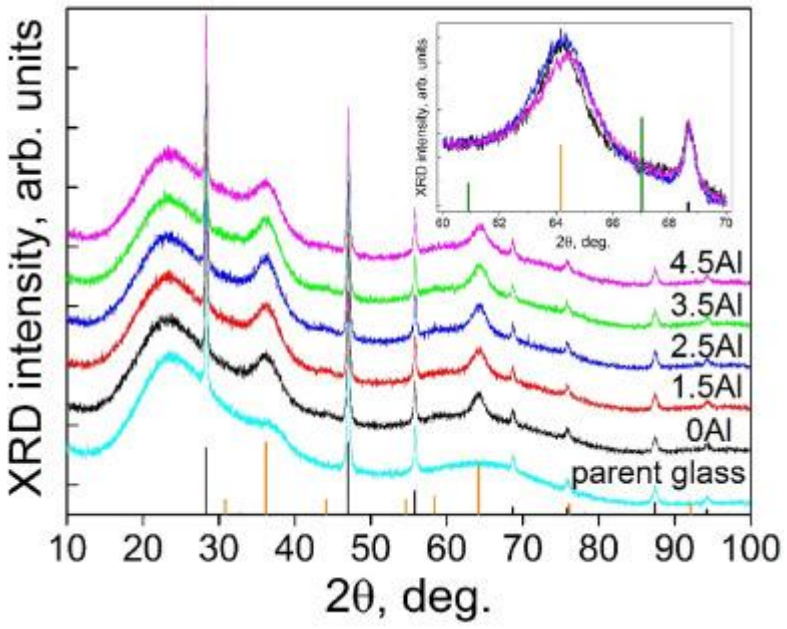

Fig. 2. XRD patterns of Al-free and Al-doped glass-ceramics in comparison with the XRD pattern of Al-free parent glass, all with the addition of 7 wt% CaF_2. The patterns are vertically shifted for clarity. The inset shows the 2θ shift of (440) reflection of the Ga-oxide spinel phase toward higher angles when Al_2O_3 content increased. The reflections of CaF_2, γ-Ga_2O_3 and γ-Al_2O_3 (inset) phases are indicated by black, orange and green sticks according to PDF files ICDD PDF2 #00-035-0816, #00-020-0426 and #00-010-0425, respectively. (For interpretation of the references to colour in this figure legend, the reader is referred to the Web version of this article.)

In our previous studies of Al-free gallium germanosilicate glasses [19], γ-Ga_2O_3 turns out to be the main crystalline phase precipitated in the bulk of the samples after treatment between T_g and the extrapolated exopeak completion temperature in DSC curves. Other studies show that small additions of NiO or TiO_2 do not change the nature of the precipitated crystalline phase but modify the temperature range of crystallization and the tendency towards devitrification [52]. Furthermore, an increase of the heat-treatment temperature leads to $LiGa_5O_8$ formation as a result of Li ions diffusion from the glass matrix into γ-Ga_2O_3 NCs [19]. The XRD patterns in Fig. 2 confirm that also in Al-doped GCs the main diffraction peaks belong to a single phase with cubic spinel-type structure.

However, a closer inspection reveals that the diffraction peaks are slightly shifted to a higher angle when increasing the Al_2O_3 content (inset in Fig. 2). Taking into account the existence of an extensive solid solution in system γ-Ga_2O_3 – γ-Al_2O_3 [24,53], the lattice constant of the spinel crystals in fabricated GCs is expected to be between the unit-cell dimensions of the end-members of the solid solutions, i.e. between 8.238 Å (the lattice constant for γ-Ga_2O_3 [31]) and 7.938 Å (the lattice constant for γ-Al_2O_3 [54]). Indeed, in our case the lattice parameter of the precipitated phase ranges from 8.21 to 8.19 Å (Table S1) when Al_2O_3 content increases from 0 to 4.5 mol%. The difference between obtained and above-mentioned values of the lattice constant for γ-Ga_2O_3 can be related to smaller NCs [55] in Al-free GCs compared to NCs in Ref. [31]. The observed change of the lattice parameter for fabricated GCs together with the absence of any diffraction line not assignable to a single cubic phase in the corresponding XRD patterns give a strong evidence of the incorporation of Al^{3+} into the γ-Ga_2O_3 phase and the formation of γ-$Ga_{2-x}Al_xO_3$ solid solutions. The cubic lattice parameter of gallia-alumina mixed oxides is reported to be an approximately linear function of the chemical composition [53,56]. This fact allows us to argue that, in the investigated range of Al_2O_3 addition, the chemical composition of the γ-$Ga_{2-x}Al_xO_3$ spinel solid solutions ranges from about γ-$Ga_{1.81}Al_{0.19}O_3$ to γ-$Ga_{1.71}Al_{0.29}O_3$ with increasing Al_2O_3 content. Thus, based on DSC and XRD data (Figs. 1 and 2, S3) we can conclude that Al_2O_3 additions used did not drastically change the sequence of phase transformation. After the exothermic process of γ-Ga_2O_3 nanocrystallization in Al-free glass, γ-Ga_2O_3 NCs transform into $LiGa_5O_8$ via diffusion-driven kinetics of Li incorporation into NCs [19] and then, at the endothermic peak, β-Ga_2O_3 forms through the decomposition of $LiGa_5O_8$. The same sequence is also valid for Al-doped glasses, except that solid solutions of Al_2O_3 in corresponding Ga-oxide compounds are formed instead of pure Ga-oxide phases.

The weight fraction of Ga-oxide spinel phase in GCs can be estimated by Rietveld-PONKCS technique described in detail in Ref. [30]. As an example, Fig. 3 shows the measured XRD pattern of 2.5Al GCs, the theoretical patterns calculated for the crystalline phases (precipitated spinel and added CaF_2) and the differential profile obtained by Rietveld method. The *R*-factors were $R_{exp} = 2.74$ and $R_{wp} = 3.82$ (the reduced chi-squared value $\chi^2 = (R_{wp}/R_{exp})^2 = 1.39$). The analysis of all GCs shows that the content of the Ga-

oxide spinel phase changes from about 14 to 20 wt% (Table S1) with a nonmonotonic dependence on the Al_2O_3 addition: the amount of the crystalline phase increases up to a maximum for 2.5Al GCs, then slightly decreases for 3.5Al GCs and finally falls to the level of Al-free GCs (~14 wt%). Taking into consideration that the fabricated glasses contain ~36-38 wt% Ga_2O_3 depending on the composition, approximately half of the total amount of Ga_2O_3 in 2.5Al GCs is segregated into the spinel NCs. As regards the nonmonotonic trend, it is in reasonable agreement with the data on density growth after the heat treatment (Fig. S4) and reflects the suggestion that an increase of glass crystallization tendency, as noted above in the DSC analysis, is offset by constant conditions of the isothermal heat treatment. In fact, a significant T_g growth at increasing Al_2O_3 addition results in a narrower range between treatment and glass transition temperature (i.e. 640°C-T_g in Fig. 1) and forces the crystallization to proceed at higher viscosity. Besides this effect, it is to be noted that another concomitant mechanism can contribute to the nonmonotonic dependence of crystallized Ga-oxide amount on the Al_2O_3 addition. The occurrence of native Ga-rich nanoheterogeneities and even native crystalline segregates (as observed in 4.5Al parent glass) may hinder the formation of new crystals [57]. This process would also explain, in fact, the unexpected low crystalline content in 4.5Al GCs. Importantly, the obtained values of crystallized fraction, taken together with the chemical composition of the spinel solid solutions and the total amount of Al_2O_3 content, indicate that Al ions in Al-doped glasses are distributed between the residual glass and the native amorphous nanoheterogeneities, wherein spinel NCs are formed [58]. This conclusion is also supported by the TEM analysis, the results of which are discussed below.

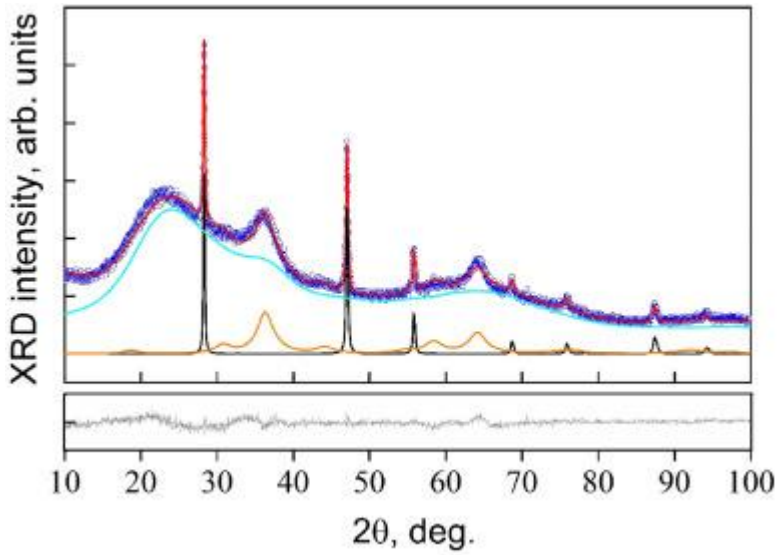

Fig. 3. Rietveld-based analysis of the XRD data for the glass-ceramics doped with 2.5 mol% Al_2O_3. Observed and calculated intensities are represented by open circles and solid curves, respectively. The solid curves are for glassy (cyan) and two crystalline phases: Ga-oxide spinel phase (orange) and fluorite (black), and also for the sum of the individual phase calculated patterns (red). The plot at the bottom of the Figure represents the difference between intensities of experimental (blue) and total calculated (red) patterns on the same scale

Fig. 4 reports TEM images, electron diffraction patterns and NP size statistics of representative samples of the investigated GC materials. The electron diffraction patterns and high-resolution TEM images, as well as the XRD data, indicate the presence of a crystalline phase in the heat-treated glasses. The electron diffraction patterns of the selected areas consist of several rings: the spotty rings resulted from the preferentially oriented spinel nanocrystallites and the diffused rings originated from the glassy phase. When moving from Al-free GCs to the sample with 2.5 mol% Al_2O_3, broader diffraction rings appear consistent with the precipitation of smaller NCs. The mean size of NPs from the analysis of the TEM images varies from about 6 nm (Al-free) to 5 nm (Al-doped) and is in reasonable agreement with NC sizes evaluated by XRD (Table S1). Since XRD peak width analysis yields volume-weighted mean size values, which are inherently different from the arithmetic mean length size calculated from TEM images [59], some discrepancy is always expected.

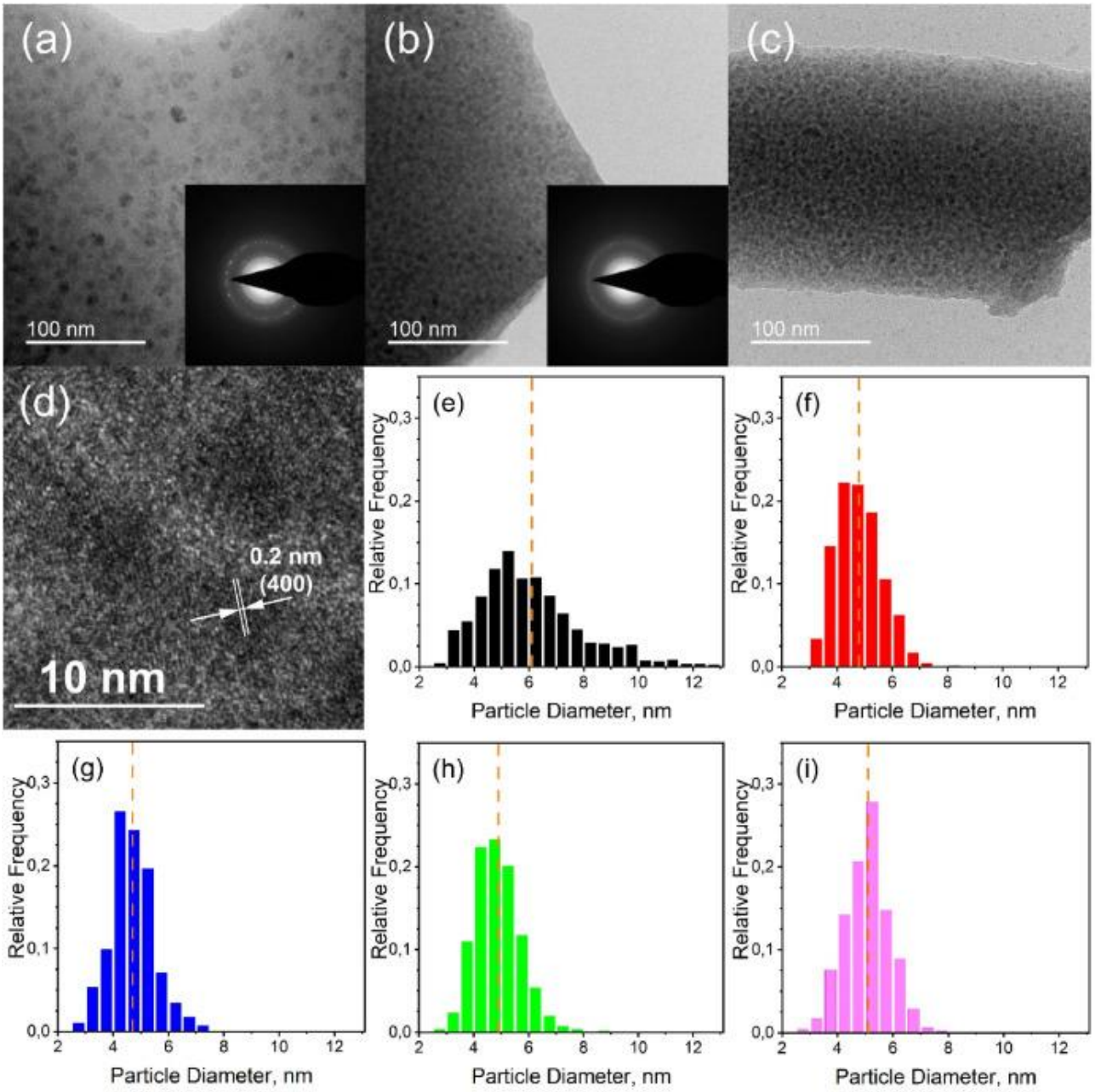

Fig. 4. TEM analysis of Al-free and Al-doped glasses heat-treated at 640 °C for 15 min. TEM images of the representative samples: (a) Al-free glass-ceramics, (b) and (c) – the glass-ceramics doped with 2.5 and 4.5 mol% Al_2O_3, respectively. The insets are the electron diffraction patterns, which were obtained from the same area in the left part of the corresponding bright-field images. (d) Typical high-resolution TEM image showing crystalline features corresponding to the lattice parameters of spinel-like Ga-oxide. From (e) to (i), histograms of NP size statistics from the analysis of the TEM images of the glass-ceramics doped with different Al_2O_3 content: 0 (e), 1.5 (f), 2.5 (g), 3.5 (h), 4.5 (i). Orange dashed lines indicate mean NP size.

A larger crystallization rate evidenced by a narrower temperature range of crystallization and sharper more intense exopeaks for Al-doped glasses has to change the size and number of NCs in fabricated GCs as revealed by the XRD data. The TEM images (Fig. 4a–c) clearly indicate that the sub-microstructure of the heat-treated Al-doped glasses is significantly different from Al-free GCs. As follows from the TEM analysis (Fig. 4e–i), Al_2O_3 addition results in narrower size distribution – which favors high optical transmittance [60] – and smaller mean NC diameter, which greatly affects NC number density. The latter quantity increases for all heat-treated Al-doped glasses since they contain more (1.5–3.5Al) or practically the same (4.5Al) content of the crystalline phase as compared to Al-free GCs. Such an increase of NC number density – influenced not only by the Al_2O_3 amount but also by decreasing nucleation barrier due to the shortening of interval 640°C-T_g, as in the case of crystallized fraction change, – implies the enhancement of nucleation in Al-doped glasses. The analysis of element distribution studied by STEM-EDX (Fig. 5) gives further insight on the role of Al_2O_3 in the crystallization process. Precipitated NPs, as expected, turned out to be rich in Ga^{3+}, while Si^{4+} distribution is opposite to that of Ga^{3+} ions. Importantly, the elemental mapping provides direct evidence of the presence of Al^{3+} inside NPs (Fig. 5). However, a significant part of Al ions is also found at the NP interface with some amount in the glassy phase. Thus, the overall effect of Al_2O_3 content on the sub-microstructure of GCs originates from a counter play between the enhanced efficiency of nucleation, probably caused by a decrease in crystalline/glassy interfacial energy, and the inhibition of crystal growth due to a viscosity increase and the accumulation of the additive at the crystallization front. As a result, the crystalline phase amount reaches the maximum for intermediate additive content (2.5 mol% Al_2O_3), and NP (NC) sizes are smaller in all Al-doped GCs compared to Al-free sample. It is worth noting that the smallest NPs are observed in 2.5Al GCs, while higher Al_2O_3 content results in slightly larger mean NP sizes (Fig. 4) at practically constant NC size (from XRD analysis), suggesting core-shell structure of precipitated NPs. This observation supposes a pronounced tendency to phase separation of the parent glasses with 3.5 and 4.5 mol% Al_2O_3, in which chemical differentiation and nanostructuring are intensified on melt cooling but crystal growth during subsequent heat treatment is suppressed by above-mentioned reasons. This assumption on increasing the degree of phase separation in 3.5

and 4.5Al glasses is confirmed by the analysis of the optical absorption spectra in the next section.

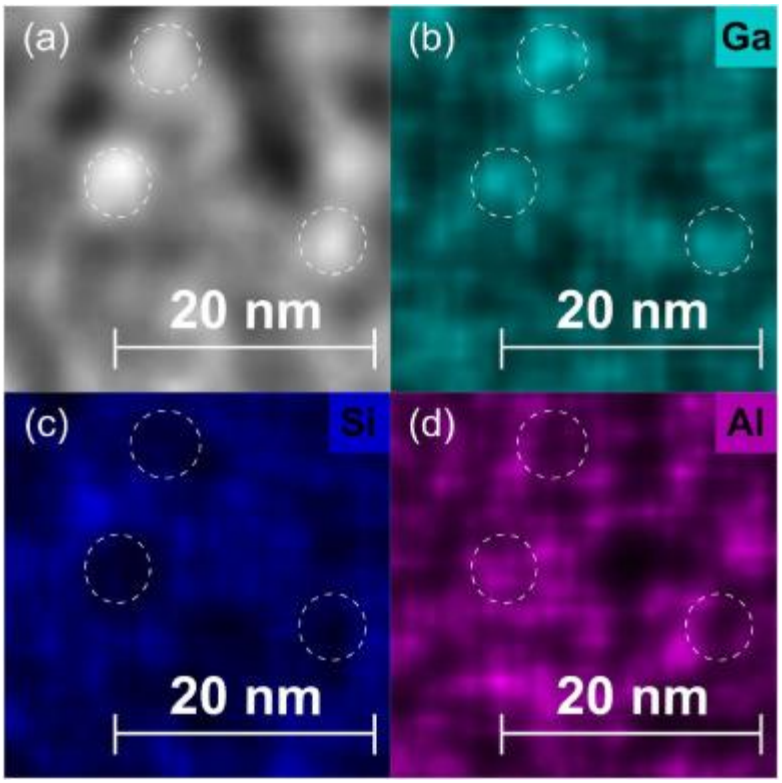

Fig. 5. Typical HAADF-STEM image of the glass-ceramics doped with 4.5 mol% Al_2O_3 (a), as an example, and the corresponding STEM-EDX mappings for Ga^{3+} (b), Si^{4+} (c) and Al^{3+} (d).

3.3. Absorption spectra of parent and heat-treated glasses

The parent and heat-treated glasses are highly transparent with an external transmittance of ~80% for ~2 mm thick samples in the spectral region near the maximum of luminescence band (about 450 nm) (Fig. S5). The absorption spectra in Fig. 6 highlight three main facts. First of all, the absorption edge shifts towards longer wavelengths upon heating at 640 °C. The absorption edge in the glass of Al-free composition has reliably been ascribed to Ge-containing Ga-oxide nanoheterogeneities with an optical gap wider than that in precipitated γ-Ga_2O_3 NCs [61]. Such native nanoheterogeneities, as evidenced before by small-angle neutron scattering data [58], are formed through liquid-liquid phase separation. The segregation of Ga-oxide from the native nanoheterogeneities, accompanied by their composition change and, consequently, the edge shift, leads to the precipitation of spinel NCs [58,61]. Since the amorphous phase separation is typical for gallium (aluminum) silicate [62], alkali gallium (aluminum) silicate [22,63] and to a lesser

extent for gallium germanate systems [40,64], it definitely occurs in our Al-doped glasses as well. As a result, the occurrence of Ga-oxide rich nanoheterogeneities determines the limit of UV transparency of the parent glasses.

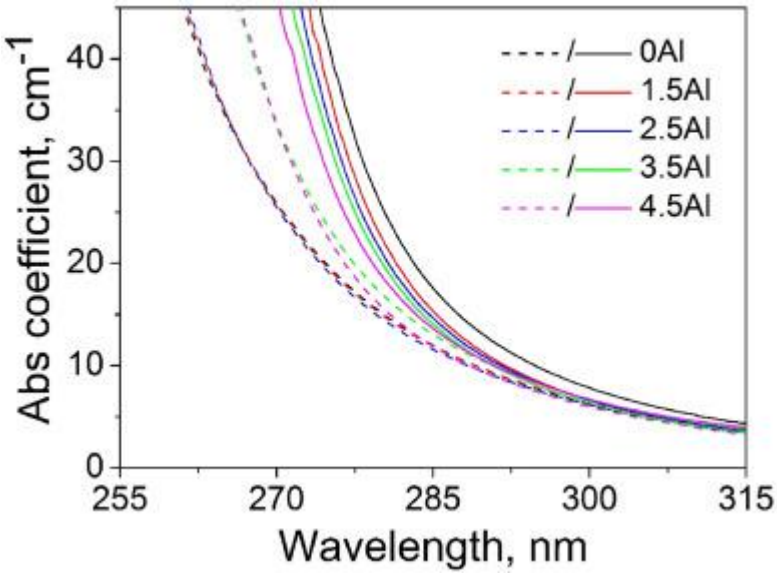

Fig. 6. Absorption spectra of Al-free and Al-doped samples: the parent glasses (dashed lines) and glass-ceramics (full lines).

The second fact is the edge shift towards shorter wavelengths in GCs when increasing Al_2O_3 content. This fact is probably related to the incorporation of Al ions into γ-Ga_2O_3 NCs. In fact, the band gap of γ-Al_2O_3 is about 7.4 eV [65], much wider than that in γ-Ga_2O_3 phase (~4.4–5.6 eV [[65], [66], [67]]). Hence, Al-doping is expected to cause a blue-shift of the intrinsic absorption edge, consistently with the absorption spectra in Fig. 6, the TEM data and the results of the XRD analysis on solid-solution formation.

Third relevant outcome deserving consideration is that the parent glasses demonstrate different spectral position of the absorption edge, implying various extent of the phase separation, caused by different glass forming ability depending on Al_2O_3 content. Specifically, 3.5Al and 4.5Al glasses show an absorption edge definitely different compared to the other glass samples and quite similar to those of GCs. This fact suggests that chemical differentiation in 3.5Al and 4.5Al glasses leads to the formation of submicroscopic regions with intermediate composition between spinel NCs and the initial Ga-oxide rich nanoheterogeneities formed in Al-free, 1.5 and 2.5Al glass samples. Interestingly, there is a small but clear difference in the slope of the edge between 3.5 and

4.5Al glasses (Fig. 6), that points to a more ordered structure of the submicroscopic regions in the case of 4.5Al glass. Its steeper slope is consistent with the fact that this glass begins to crystallize on melt cooling with the precipitation of a minor amount of the Ga-oxide spinel phase according to the XRD analysis (Fig. S1). Some support of the validity of the above-mentioned interpretations can be found in TEM images and electron diffraction patterns of the parent glasses (Fig. S2). Despite the low electron density difference between gallium germanosilicate matrix and Ge-containing Ga-oxide nanoheterogeneities, some contrast features are detected in TEM images when increasing Al_2O_3 content up to 4.5 mol%. Additionally, the electron diffraction pattern of 4.5Al sample exhibited sharper rings indicative of crystalline domain formation compared to the other two samples. This fact is in good agreement with the XRD data of the parent glasses, and both observations indicate that the addition of Al_2O_3 and the increase of its content intensify chemical differentiation and nanostructuring in the parent glasses. Further insight into the role of Al_2O_3 in the optical response of GCs can be obtained by joining the data on their sub-microstructure with the study of nanophase light emission.

3.4. Photoluminescence of glass-ceramics

The fabricated GC materials display an intense and broad room-temperature luminescence excited at photon energy higher than the onset of the UV absorption tail in Fig. 6. The light-emission and excitation patterns of these materials are reported in Fig. 7a–e and comprise three main contributions in the UV, blue and green spectral regions, all ascribable to the luminescence of Ga-oxide materials [68,69]. The main «blue» PL component, centered at around 450 nm, is usually attributed to the radiative recombination of DAPs formed by native structural defects [70]. The donor states are ascribed to oxygen vacancies $V_O^{\cdot}$ and the acceptor states to oxygen and gallium vacancies in $(V_O, V_{Ga})'$ sites [68]. Additional «green» component at about 530 nm, whose intensity is enhanced in the single crystal β-Ga_2O_3 grown under O_2 atmosphere [71], arises from transitions related to localized defect sites, probably interstitial oxygen atoms with a minor contribution of gallium vacancies [72]. As regards the minor «UV» component observed at about 350 nm, it is attributed to exciton-like transitions [73].

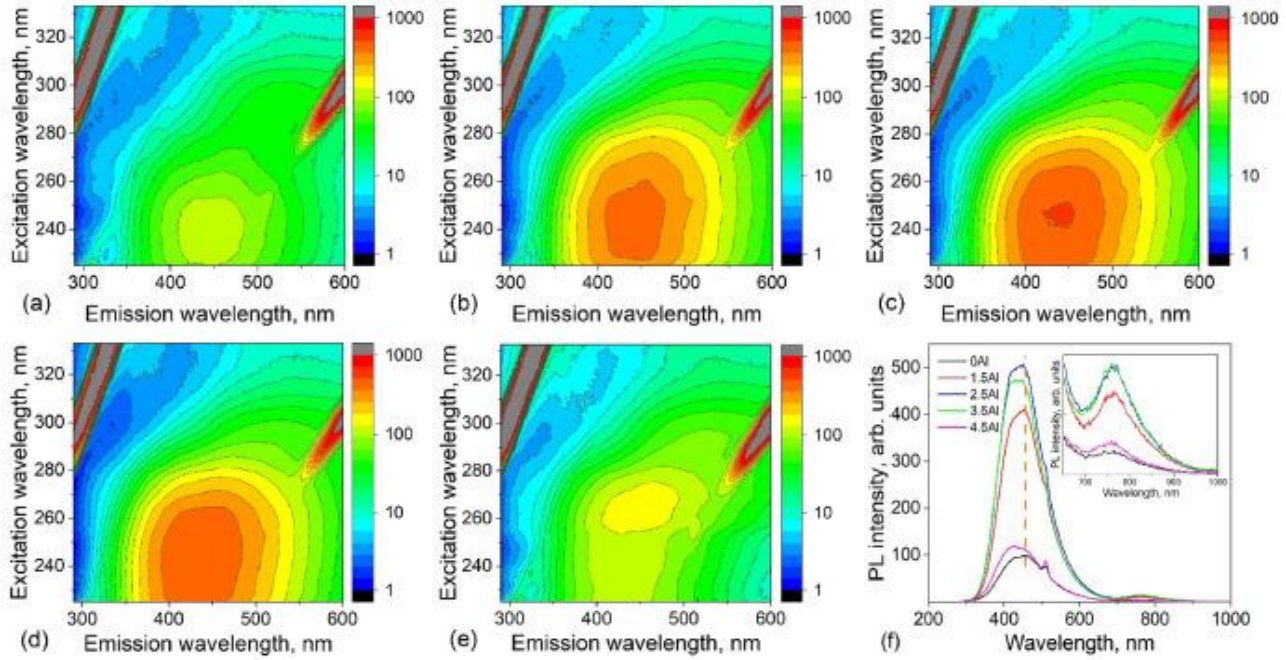

Fig. 7. (a–e) Contour plots of PL intensity as a function of emission and excitation wavelength in the glass-ceramics doped with different Al_2O_3 content: 0 (a), 1.5 (b), 2.5 (c), 3.5 (d) and 4.5 (e). The intense features linearly dependent on the wavelength in the upper part of the contour plots are due to the excitation light at the first and second order. (f) Spectral distribution of light emission at the excitation wavelength of 250 nm providing the most intense PL according to the contour plots and an enlarged part of the PL spectra in the spectral range of 650–1000 nm (inset). Orange dashed line represents the position of PL band maximum for Al-free glass.

The contour plots in Fig. 7 confirm that the main light emission in the investigated materials is the blue band centered at about 450 nm and excited at about 250 nm. Fig. 7f reports representative emission spectra extracted from the 3D patterns at the indicated excitation and extended to the long wavelength region so as to include the low-intensity band peaked at about 760 nm (inset in Fig. 7f). Photoluminescence bands in this spectral region are often observed in oxides as a result of light emission from non-bridging oxygen sites. The detection of such a band in investigated GCs is expected because of the formation of a glass-crystal interface, which implies the occurrence of a number of coordination defects, including non-bridging oxygen, from the structural mismatch between crystalline and glassy phases. The dependence of the 760 nm band intensity on

Al_2O_3 addition (inset in Fig. 7f) indeed supports this interpretation since an indirect effect of Al_2O_3 addition on non-bridging oxygen concentration is expected. In fact, the Al_2O_3 addition influences the amount of crystallized phase and the NC size, with consequent effects on the interface formation. As a result, the GC samples with the largest crystallized fractions (2.5 and 3.5Al) display the most intense «red» emission (consistent with the most extended interface), while the samples with lower crystallinity (0 and 4.5Al) show considerably weaker PL signals.

As regards the blue band, the PL data register a not negligible effect of Al_2O_3 addition on both spectral position and light emission intensity. The spectral position shifts towards higher energies when Al_2O_3 content is increased, consistently with the widening of the band gap (Fig. 6). About the PL intensity, the spectra in Fig. 7f show a relevant nonmonotonic change with the Al_2O_3 concentration: the PL signal increases with Al_2O_3 content until it reaches its maximum for GCs with 2.5 mol% Al_2O_3 and then decreases. This behaviour suggests some relation with the nonmonotonic change of crystallized Ga-oxide amount evidenced by the XRD analysis of the GC samples. More specifically, we find that the integrated emission intensity in Fig. 7f appears to follow, to some extent, the change of NC number density, which we can estimate from the mean NC (NP) size, the value of crystallized fraction and the density of GCs according to the TEM data, XRD analysis and density measurements, respectively (see Fig. 8a, Table S1). This result points to the importance of thermal treatment and additive content as the main factor for maximizing NC number density and, consequently for improving the light emission properties.

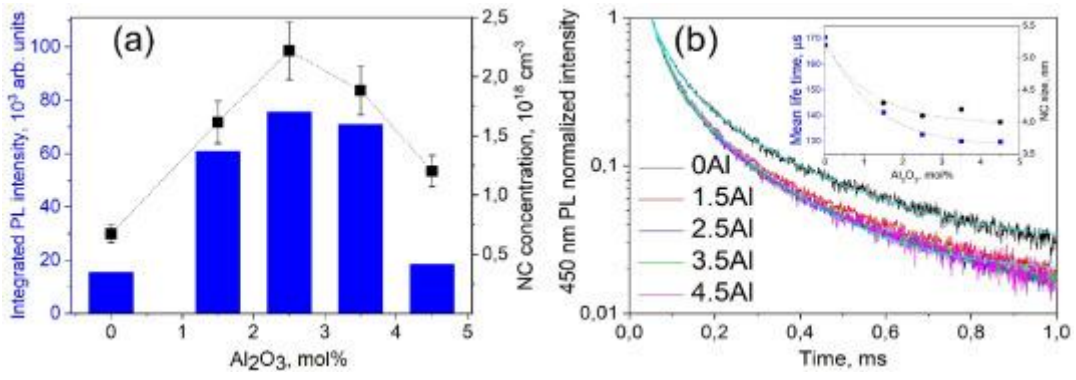

Fig. 8. (a) Dependence of integrated emission intensity (from integration of spectra in Fig. 7f) and NC concentration on Al_2O_3 content in the glass-ceramics. (b) Time decay of PL at 450 nm in the glass-ceramics and, as an example, fitting curves for Al-free and 4.5Al samples. Inset: influence of Al_2O_3 addition on mean lifetime in the ms regime and NC size. Dashed lines in (a) and in the inset are guides for the eyes.

Other factors can however play a role, contributing to the resulting Al_2O_3 dependence of the 450 nm PL band intensity. Some evidence appears in 2.5Al and 4.5Al samples – in the former, the integrated intensity is larger than that expected from the increase of NC concentration, and in the latter a large intensity fall is detected which is not fully justified by the lowering of NC number density. More detailed evidence comes from PL lifetime data.

Fig. 8b reports PL decay curves, in the ms time range, of the 450 nm blue emission excited at 250 nm in the investigated set of GCs. As reported in the inset of Fig. 8b, the PL lifetime turns out to be progressively shortened by Al_2O_3 addition and, indeed, this result is also found in the ns and μs ranges (Figs. S6 and S7). The lifetime shortening can be the result of two kinds of possibly concurrent effects. On the one hand, a reduced mean distance between donors and acceptors in the DAP recombination process (possibly caused by the decrease of mean NC size, as evidenced by the XRD and TEM data, and/or an increase of donor and/or acceptor sites per NC) is expected to shorten the lifetime. In principle, it could increase the radiative recombination rate and the PL intensity, even if, actually, the PL intensity can also be determined by possible changes of donor and acceptor concentration, as observed in similar systems [74]. On the other hand, an increase of nonradiative channels (possibly arising by a larger amount of nonradiative recombination sites at larger Al_2O_3 addition) can be another source of lifetime shortening, which gives rise to a decrease of PL intensity. The latter effect probably contributes to the lifetime shortening at Al_2O_3 content larger than 2.5 mol%. In fact, no increase of donor and acceptor concentration – as a possible factor causing a lifetime shortening – is indeed expected at large Al_2O_3 content, when the NC size is observed not to change sensibly (with even an increase of NP size) and when progressive Ga^{3+} substitution by Al^{3+} ions should hinder the formation of defect sites. The calculated formation energy of intrinsic defects,

such as donor and acceptor sites, in Al-doped Ga_2O_3 is in fact larger than in Al-free material [75], and can rather be a concurrent cause of PL intensity reduction. As a result, not only is the sub-microstructure influenced by Al-doping, but also the overall PL efficiency of GCs is affected (Fig. 7, Fig. 8) because of multiple factors. They comprise modifications of the sub-microstructure itself, through changes of concentration and mean size of NCs, but also include the formation of nonradiative recombination sites and a possible decrease of donor and acceptor concentration.

Indeed, the occurrence of competitive Al_2O_3 effects on the blue PL emission can also explain some results of a previous study reporting no enhancement of blue PL intensity in similar GCs – but with distinct composition comprising a magnesium-alkali-silicate matrix – despite both crystallized fraction and Ga-oxide NC number density turn out to increase with Al_2O_3 addition [16]. In fact, our data show that the addition of 4.5 mol% Al_2O_3, which is about the minimum Al_2O_3 content in Ref. [16], is already too large for keeping PL enhancement mechanisms still dominant on the detrimental effects of Al_2O_3 addition, giving rise to basically the same PL intensity of Al-free GCs. This outcome suggests that a larger amount of Al_2O_3 probably causes small or negligible PL enhancement because of dominant effects of nonradiative decay channels and/or a possible reduction of radiative recombination sites. The addition of MgO, with a resulting heterovalent Mg^{2+} doping of NCs, could in fact favor an effective lowering of recombination sites [76], as already observed in Ni^{2+}-doped gallium germanosilicates [18].

4. Conclusion

In summary, additions of Al_2O_3 (from 1.5 to 4.5 mol%) to low-alkali gallium germanosilicate glasses lead to the formation of γ-$Ga_{2-x}Al_xO_3$ spinel nanocrystals with a significant change in the microstructure of the fabricated glass-ceramics. The DSC analysis demonstrates that Al_2O_3 added over 100% turns out to facilitate the melting process and the subsequent crystallization of γ-Ga_2O_3-based solid solutions. At fixed heat treatment temperature, the addition of Al_2O_3 up to 2.5–3.5 mol% promotes glass crystallization even at a moderate increase of glass viscosity. As a result, the integrated luminescence intensity of the glass-ceramics is enhanced up to a factor of five with respect

to Al-free heat-treated glass without losing initial high transparency. The effect can be mainly ascribed to the increase of NC concentration and the parallel narrowing of NC size distribution. The monotonic shortening of the PL decay time with Al_2O_3 content suggests that the increase of NC number density and NC size reduction are accompanied by the parallel promotion of competitive mechanisms, such as nonradiative decay channels and a decrease of donor and acceptor species.

Acknowledgements

This study was supported by the Russian Foundation for Basic Research (RFBR), project number 20-03-00809. The authors wish to thank A.A. Maurus for his assistance in the glass fabrication and Dr. A. Lotnyk and N. Braun for their help in electron microscopy investigations. A.S. Lipatiev acknowledges scholarship support with in the program "Mikhail Lomonosov" by German Acadamic Exchange Service (DAAD) and Ministry of Science and Higher Education of the Russian Federation.

References

[1] W. Holand, G.H. Beall, Glass-Ceramic Technology 3rd (Eds.), Wiley-American Ceramic Society (2019)

[2] R. Ya **Khodakovskaya, Chemistry of Titanium-Containing Glasses and Glass Ceramics** Chemistry, Moscow (1978)

[3] T.I. Barry, J.M. Cox, R. Morrell **Cordierite glass-ceramics – effect of TiO_2 and ZrO_2 content on phase sequence during heat treatment** J. Mater. Sci., 13 (1978), pp. 594-610, 10.1007/BF00541810

[4] G.H. Chen, X.Y. Liu **Sintering, crystallization and properties of MgO-Al_2O_3-SiO_2 system glass-ceramics containing ZnO** J. Alloys Compd., 431 (2007), pp. 282-286, 10.1016/j.jallcom.2006.05.060

[5] A. Hunger, G. Carl, C. Rüssel **Formation of nano-crystalline quartz crystals from ZnO/MgO/Al_2O_3/TiO_2/ZrO_2/SiO_2 glasses** Solid State Sci., 12 (2010), pp. 1570-1574, 10.1016/j.solidstatesciences.2010.06.025

[6] I. Alekseeva, O. Dymshits, M. Tsenter, A. Zhilin **Influence of various alkali and divalent metal oxides on phase transformations in NiO-doped glasses of the Li_2O-Al_2O_3-SiO_2-TiO_2 system** J. Non-Cryst. Solids, 357 (2011), pp. 2209-2214, 10.1016/j.jnoncrysol.2010.12.065

[7] K. Thieme, C. Rüssel **Nucleation inhibition despite lower glass viscosities? – effect of the B_2O_3, Na_2O and K_2O addition on the crystallization behavior of lithium disilicate glasses** Ceram. Int., 43 (2017), pp. 9644-9652, 10.1016/j.ceramint.2017.04.134

[8] W. Zhu, H. Jiang, H. Zhang, S. Jia, Y. Liu **Effect of TiO_2 and CaF_2 on the crystallization behavior of Y_2O_3-Al_2O_3-SiO_2 glass ceramics** Ceram. Int., 44 (2018), pp. 6653-6658, 10.1016/j.ceramint.2018.01.076

[9] Z. Gao, H. Zhu, B. Sun, Y. Ji, X. Lu, H. Tian, J. Ren, S. Guo, J. Zhang, J. Yang, X. Meng, K. Tanaka **Photonic engineering of superbroadband near-infrared emission in nanoglass composites containing hybrid metal and dielectric nanocrystals** Photon. Res., 8 (2020), pp. 698-706, 10.1364/PRJ.379662

[10] D. Chen **Near-infrared long-lasting phosphorescence in transparent glass ceramics embedding Cr^{3+}-doped $LiGa_5O_8$ nanocrystals** J. Eur. Ceram. Soc., 34 (2014), pp. 4069-4075, 10.1016/j.jeurceramsoc.2014.06.013

[11] J. Luo, B. Wu, B. Zhu, S. Zhou, H. Yang, S. Ye, G. Lakshminarayana, J. Qiu **Energy transfer between Cr^{3+} and Ni^{2+} in transparent glass ceramics containing β-Ga_2O_3 nanocrystals** J. Appl. Phys., 106 (2009), Article 053527, 10.1063/1.3195084

[12] Y.Shi, C. Gao, Q. Ye, S. Wang, Q. Wang, M. Gao, P. Loiko, N. Skoptsov, O. Dymshits, A. Zhilin, S. Zapalova, M. Tsenter, V. Vitkin, X. Mateos, K. Yumashev **Passively Q-switched 1.6 μm Er:YAG laser with a γ-Ga_2O_3:Co-based glass-ceramics as a saturable absorber** Laser Phys. Lett., 15 (2018), Article 045004, 10.1088/1612-202X/aaa9a8

[13] S. Lin, H. Lin, C. Ma, Y. Cheng, S. Ye, F. Lin, R. Li, J. Xu, Y. Wang **High-security-level multi-dimensional optical storage medium: nanostructured glass embedded with $LiGa_5O_8$:Mn^{2+} with photostimulated luminescence** Light Sci. Appl., 9 (2020), p. 22, 10.1038/s41377-020-0258-3

[14] Z. Gao, X. Lu, Y. Chu, S. Guo, L. Liu, Y. Liu, S. Sun, J. Ren, J. Yang **The distribution of rare earth ions in a γ-Ga_2O_3 nanocrystal-silicate glass composite and its influence on the photoluminescence properties** J. Mater. Chem. C, 6 (2018), pp. 2944-2950, 10.1039/C8TC00325D

[15] S. Zhou, C. Li, G. Yang, G. Bi, B. Xu, Z. Hong, K. Miura, K. Hirao, J. Qiu **Self-limited nanocrystallization-mediated activation of semiconductor nanocrystal in an amorphous solid** Adv. Funct. Mater., 23 (2013), pp. 5436-5443, 10.1002/adfm.201300969

[16] L. Lin, R. Miao, W. Xie, J. Chen, Y. Zhao, Z. Wu, J. Qiu, H. Yu, S. Zhou **In situ and tunable structuring of semiconductor-in-glass transparent composite** iScience, 24 (2021), Article 101984, 10.1016/j.isci.2020.101984

[17] B. Fernandes, M. Hegde, P.C. Stanish, Z.L. Mišković, P.V. Radovanovic **Photoluminescence decay dynamics in γ-Ga_2O_3 nanocrystals: the role of exclusion distance at short time scales** Chem. Phys. Lett., 684 (2017), pp. 135-140, 10.1016/j.cplett.2017.06.052

[18] V.N. Sigaev, N.V. Golubev, E.S. Ignat'eva, A. Paleari, R. Lorenzi **Light-emitting Ga-oxide nanocrystals in glass: a new paradigm for low-cost and robust UV-to-visible solar-blind converters and UV emitters** Nanoscale, 6 (2014), pp. 1763-1774, 10.1039/C3NR05210A

[19] N.V. Golubev, E.S. Ignat'eva, V.N. Sigaev, A. Lauria, L. De Trizio, A. Azarbod, A. Paleari, R. Lorenzi **Diffusion-driven and size-dependent phase changes of gallium oxide nanocrystals in a glassy host** Phys. Chem. Chem. Phys., 17 (2015), pp. 5141-5150, 10.1039/C4CP05485G

[20] N.V. Golubev, E.S. Ignat'eva, M.Z. Ziyatdinova, V.N. Sigaev **Optical glass with γ-Ga_2O_3 nanocrystals for UV-C radiation visualization** Glass Ceram., 77 (2021), pp. 412-414, 10.1007/s10717-021-00319-7

[21] P.L. Higby, J.C. Lapp, J.E. Shelby **Crystallization of lithium alumino/galliosilicate glasses** J. Non-Cryst. Solids, 102 (1988), pp. 125-129, 10.1016/0022-3093(88)90122-6

[22] J.E. Shelby **Alkali and alkaline earth galliosilicate glasses** Key Eng. Mater., 94–95 (1994), pp. 279-316 https://doi.org/10.4028/

[23] L. Peng, J.F. Stebbins **High resolution 17O MAS and triple-quantum** MAS NMR studies of gallosilicate glasses, J. Non-Cryst. Solids, 354 (2008), pp. 3120-128, 10.1016/j.jnoncrysol.2008.01.026

[24] L.R. Pinckney, B.N. Samson, G.H. Beall, J. Wang, N.F. Borrelli **Transparent gallate spinel glass-ceramics** Ceram. Trans., 137 (2003), pp. 265-275, 10.13140/2.1.1314.7524

[25] S. Zhou, G. Feng, B. Wu, N. Jiang, S. Xu, J. Qiu **Intense infrared luminescence in transparent glass-ceramics containing β-Ga_2O_3:Ni^{2+} nanocrystals** J. Phys. Chem. C, 111 (2007), pp. 7335-7338, 10.1021/jp068370i

[26]

O. Dymshits, V. Vitkin, I. Alekseeva, A. Khubetsov, M. Tsenter, A. Polishchuk, A. Volokitina, J.M. Serres, X. M ateos, A. Zhilin, P. Loiko **Transparent glass-ceramics based on Co^{2+}-doped γ-$Ga_xAl_{2-x}O_3$ spinel nanocrystals for passive Q-switching of Er lasers** J. Lumin., 234 (2021), Article 117993, 10.1016/j.jlumin.2021.117993

[27] E.S. Ignat'eva, N.V. Golubev, V.M. Mashinskii, A.K. Senatorov, N.V. Varapai, V.N. Sigaev **Crystallization and luminescence of Ni^{2+}-doped gallium-germanium silicate glasses with partial Al_2O_3 substitution of Ga_2O_3** Glass Ceram., 78 (2022), pp. 392-396, 10.1007/s10717-022-00418-z

[28]

N.V. Golubev, E.S. Ignat'eva, A.A. Maurus, M.Z. Ziyatdinova, E.V. Lopatina, R. Lorenzi, A. Paleari, V.N. Sigae v **Photoluminescence of gallate glass-ceramics: Al_2O_3 influence** Glass Ceram., 11 (2020), pp. 12-15 (English translation 77 (2021) 415-418, doi:10.1007/s10717-021-00320-0)

[29] J.I. Langford, A.J.C. Wilson **Scherrer after sixty years: a survey and some new results in the determination of crystallite size** J. Appl. Crystallogr., 11 (1978), pp. 102-113, 10.1107/S0021889878012844

[30] N.V.Y. Scarlett, I.C. Madsen **Quantification of phases with partial or no known crystal structures** Powder Diffr., 21 (2006), pp. 278-284, 10.1154/1.2362855

[31] H.Y. Playford, A.C. Hannon, E.R. Barney, R.I. Walton **Structures of uncharacterised polymorphs of gallium oxide from total neutron diffraction** Chem. Eur J., 19 (2013), pp. 2803-2813, 10.1002/chem.201203359

[32] **Crystallography open database** Crystallographic information file №1000043 (2022) https://www.crystallography.net/cod/1000043.html, Accessed 12th Jan 2022

[33] The British Standards Institution **BS ISO 9276-2:2014 Representation of Results of Particle Size Analysis Part 2: Calculation of Average Particle Sizes/diameters and Moments from Particle Size Distribution** (2014)

[34] J.R. Lakowicz (Ed.), Principles of Fluorescence Spectroscopy (third ed.), Springer, New York (2006)

[35] J.L. Piguet, J.E. Shelby **Transformation-range behavior of Li_2O-$(Al,Ga)_2O_3$-SiO_2 glasses** J. Am. Ceram. Soc., 68 (1985), pp. C-232-C-233, 10.1111/j.1151-2916.1985.tb15794.x

[36] A. Buri, D. Caferra, F. Branda, A. Marotta **Relationship between composition and glass transition temperature in Na_2O-M_2O_3-SiO_2 glasses (M= Ga, In, Sc, Y, La)** Phys. Chem. Glasses, 23 (1982), pp. 37-40

[37] P.L. Higby, J.E. Shelby, J.C. Phillips, A.D. Legrand **EXAFS study of alkali galliosilicate glasses** J. Non-Cryst. Solids, 105 (1988), pp. 139-148, 10.1016/0022-3093(88)90348-1

[38] D.M. Zirl, S.H. Garofalini **Structure of sodium aluminosilicate glasses** J. Am. Ceram. Soc., 73 (1990), pp. 2848-2856, 10.1111/j.1151-2916.1990.tb06685.x

[39] C.I. Merzbacher, D.A. McKeown **X-ray absorption studies of Ge and Ga environments in BaO-Ga_2O_3-GeO_2 glasses** J. Non-Cryst. Solids, 162 (1993), pp. 81-100, 10.1016/0022-3093(93)90743-H

[40] J.M. Jewell **Alkaline earth gallogermanate glasses** Key Eng. Mater., 94–95 (1994), pp. 317-344 https://doi.org/10.4028/

[41] N.H. Ray **Composition – property relationships in inorganic oxide glasses** J. Non-Cryst. Solids, 15 (1974), pp. 423-434, 10.1016/0022-3093(74)90148-3

[42] M. Saad, M. Poulain **Glass forming ability criterion** Mater. Sci. Forum, 19–20 (1987), pp. 11-18 https://doi.org/10.4028/www.scientific.net/MSF.19-20.11

[43] M.L.F. Nascimento, L.A. Souza, E.B. Ferreira, E.D. Zanotto **Can glass stability parameters infer glass forming ability?** J. Non-Cryst. Solids, 351 (2005), pp. 3296-3308, 10.1016/j.jnoncrysol.2005.08.013

[44] A. Kozmidis-Petrovic, J. Šesták **Forty years of the Hrubý glass-forming coefficient via DTA when comparing other criteria in relation to the glass stability and vitrification ability** J. Therm. Anal. Calorim., 110 (2012), pp. 997-1004, 10.1007/s10973-011-1926-6

[45] S.K. Dubrovo **Acid resistance of alkali-aluminosilicate and galliosilicate glasses** Glass Phys. Chem., 4 (1978), pp. 396-400

[46] B. Zhao, E. Jak, P.C. Hayes **The effect of Al_2O_3 on liquidus temperatures of fayalite slags** Metall. Mater. Trans. B, 30 (1999), pp. 597-605, 10.1007/s11663-999-0020-y

[47] B.N. Samson, L.R. Pinckney, J. Wang, G.H. Beall, N.F. Borrelli **Nickel-doped nanocrystalline glass-ceramic fiber** Opt. Lett., 27 (2002), pp. 1309-1311, 10.1364/OL.27.001309

[48] Z. Huang, L. Wu **Phase Equilibria Diagrams of High-Temperature Non-oxide Ceramics** Springer, Singapore (2018)

[49] C.W.W. Hoffman, J.J. Brown **Compound formation and Mn^{2+}-activated luminescence in the binary systems R_2O- and RO-Ga_2O_3** J. Inorg. Nucl. Chem., 30 (1968), pp. 63-79, 10.1016/0022-1902(68)80064-8

[50] S. Bhattacharyya, C. Bocker, T. Heil, J.R. Jinschek, T. Höche, C. Rüssel, H. Kohl **Experimental evidence of self-limited growth of nanocrystals in glass** Nano Lett., 9 (2009), pp. 2493-2496, 10.1021/nl901283r

[51] N.V. Golubev, E.S. Ignat'eva, V.M. Mashinsky, E.O. Kozlova, V.N. Sigaev, A. Monguzzi, A. Palearia, R. Lorenzi **Pre-crystallization heat treatment and infrared luminescence enhancement in Ni^{2+}-doped transparent glass-ceramics** J. Non-Cryst. Solids, 515 (2019), pp. 42-49, 10.1016/j.jnoncrysol.2019.04.006

[52] A. Paleari, N.V. Golubev, E.S. Ignat'eva, V.N. Sigaev, A. Monguzzi, R. Lorenzi **Donor-acceptor control in grown-in-glass gallium oxide nanocrystals by crystallization-driven heterovalent doping** ChemPhysChem, 18 (2017), pp. 662-669, 10.1002/cphc.201601247

[53] C.O. Areán, M.R. Delgado, V. Montouillout, D. Massiot **Synthesis and characterization of spinel-type gallia-alumina solid solutions** Z. Anorg. Allg. Chem., 631 (2005), pp. 2121-2126, 10.1002/zaac.200570027

[54] L. Smrčok, V. Langer, J. Křestan **γ-Alumina: a single-crystal X-ray diffraction study** Acta Crystallogr., Sect. C: Cryst. Struct. Commun., 62 (2006), pp. i83-i84, 10.1107/S0108270106026850

[55] H.Y. Playford, A.C. Hannon, M.G. Tucker, D.M. Dawson, S.E. Ashbrook, R.J. Kastiban, J. Sloan, R.I. Walton

Characterization of structural disorder in γ-Ga_2O_3 J. Phys. Chem. C, 118 (2014), pp. 16188-16198, 10.1021/jp5033806

[56] D.S. Cook, J.E. Hooper, D.M. Dawson, J.M. Fisher, D. Thompsett, S.E. Ashbrook, R.I. Walton **Synthesis and polymorphism of mixed aluminum-gallium oxides** Inorg. Chem., 59 (2020), pp. 3805-3816, 10.1021/acs.inorgchem.9b03459

[57] V.M. Fokin, O.V. Potapov, C.R. Chinaglia, E.D. Zanotto **The effect of pre-existing crystals on the crystallization kinetics of a soda-lime-silica glass. The courtyard phenomenon** J. Non-Cryst. Solids, 258 (1999), pp. 180-186, 10.1016/S0022-3093(99)00417-2

[58] V.N. Sigaev, N.V. Golubev, E.S. Ignat'eva, B. Champagnon, D. Vouagner, E. Nardou, R. Lorenzi, A. Paleari **Native amorphous nanoheterogeneity in gallium germanosilicates as a tool for driving Ga_2O_3 nanocrystal formation in glass for optical devices** Nanoscale, 5 (2013), pp. 299-306, 10.1039/C2NR32790B

[59] H. Borchert, E.V. Shevchenko, A. Robert, I. Mekis, A. Kornowski, G. Grübel, H. Weller **Determination of nanocrystal sizes: a comparison of TEM, SAXS, and XRD studies of highly monodisperse $CoPt_3$ particles** Langmuir, 21 (2005), pp. 1931-1936, 10.1021/la0477183

[60] P.A. Tick **Are low-loss glass-ceramic optical waveguides possible?** Opt. Lett., 23 (1998), pp. 1904-1905, 10.1364/OL.23.001904

[61] A. Paleari, V.N. Sigaev, N.V. Golubev, E.S. Ignat'eva, S. Bracco, A. Comotti, A. Azarbod, R. Lorenzi **Crystallization of nanoheterogeneities in Ga-containing germanosilicate glass: dielectric and refractive response changes** Acta Mater., 70 (2014), pp. 19-29, 10.1016/j.actamat.2014.02.022

[62] V.I. Averjyanov, M.P. Areshev **Immiscibility regions in refractory glass forming systems Ga_2O_3-SiO_2, Al_2O_3-SiO_2 and Al_2O_3-Ga_2O_3-SiO_2** Fiz. Khim. Stekla, 15 (1989), pp. 846-853 (in Russian)

[63] F.Ya Galakhov, V.I. Averjyanov, V.T. Vavilonova, M.P. Areshev **Immiscibility regions in systems Li_2O-Al_2O_3(Ga_2O_3)-SiO_2** Fiz. Khim. Stekla, 9 (1983), pp. 745-748 (in Russian)

[64] N.G. Gutkina, I.I. Kozhina, L.K. Shmatok **Vitrification and crystallization in ternary germanate-lanthanum systems with gallium and boron oxides** Izv. Akad. Nauk. SSSR - Neorganicheskiye Mater., 11 (1975), pp. 721-725 (in Russian)

[65] T. Oshima, Y. Kato, E. Magome, E. Kobayashi, K. Takahashi **Characterization of pseudomorphic γ-Ga_2O_3 and γ-Al_2O_3 films on $MgAl_2O_4$ substrates and the band-alignment at the coherent γ-Ga_2O_3/Al_2O_3 heterojunction interface** Jpn. J. Appl. Phys., 58 (2019), Article 060910, 10.7567/1347-4065/ab219f

[66] C.C. Huang, C.S. Yeh **GaOOH, and β-and γ-Ga_2O_3 nanowires: preparation and photoluminescence** New J. Chem., 34 (2010), pp. 103-107, 10.1039/B9NJ00392D

[67] H. Kan, W. Zheng, C. Fu, R. Lin, J. Luo, F. Huang **Ultrawide band gap oxide nanodots (Eg > 4.8 eV) for a high-performance deep ultraviolet photovoltaic detector** ACS Appl. Mater. Interfaces, 12 (2020), pp. 6030-6036, 10.1021/acsami.9b17679

[68] L. Binet, D. Gourier **Origin of the blue luminescence of β-Ga_2O_3** J. Phys. Chem. Solid., 59 (1998), pp. 1241-1249, 10.1016/S0022-3697(98)00047-X

[69] R. Lorenzi, A. Paleari, N.V. Golubev, E.S. Ignat'eva, V.N. Sigaev, M. Niederberger, A. Lauria **Non-aqueous sol-gel synthesis of hybrid rare-earth-doped γ-Ga_2O_3 nanoparticles with multiple organic-inorganic-ionic light-emission features** J. Mater. Chem. C, 3 (2015), pp. 41-45, 10.1039/C4TC02118E

[70] T. Wang, P.V. Radovanovic ***In situ*** **enhancement of the blue photoluminescence of colloidal Ga_2O_3 nanocrystals by promotion of defect formation in reducing conditions** Chem. Commun., 47 (2011), pp. 7161-7163, 10.1039/C1CC11957E

[71] E.G. Villora, T. Atou, T. Sekiguchi, T. Sugawara, M. Kikuchi, T. Fukuda **Cathodoluminescence of undoped β-Ga_2O_3 single crystals** Solid State Commun., 120 (2001), pp. 455-458, 10.1016/S0038-1098(01)00409-4

[72] Q.D. Ho, T. Frauenheim, P. Deák **Origin of photoluminescence in β-Ga_2O_3** Phys. Rev. B, 97 (2018), Article 115163, 10.1103/PhysRevB.97.115163

[73] S. Yamaoka, M. Nakayama **Evidence for formation of self-trapped excitons in a β-Ga_2O_3 single crystal** Phys. Status Solidi C, 13 (2016), pp. 93-96, 10.1002/pssc.201510124

[74] T. Wang, P.V. Radovanovic **Size-dependent electron transfer and trapping in strongly luminescent colloidal gallium oxide nanocrystals** J. Phys. Chem. C, 115 (2011), pp. 18473-18478, 10.1021/jp205502d

[75] X. Ma, Y. Zhang, L. Dong, R. Jia **First-principles calculations of electronic and optical properties of aluminum-doped β-Ga_2O_3 with intrinsic defects** Results Phys., 7 (2017), pp. 1582-1589, 10.1016/j.rinp.2017.04.023

[76] S.-Y. Chu, T.-H. Yeh, C.-T. Lee, H.-Y. Lee **Mg-doped beta-Ga_2O_3 films deposited by plasma-enhanced atomic layer deposition system for metal-semiconductor-metal ultraviolet C photodetectors** Mater. Sci. Semicond. Process., 142 (2022), Article 106471, 10.1016/j.mssp.2022.106471